Research paper

Preparation and Performance of CL-20-based Ultraviolet-curable High-explosive Ink and Its Application in Rigid Explosive Networks by Direct Ink Writing

Rui Li[1], **Weibing Li**[1,*], **Xiaode Guo**[2], **Li Liang**[2], **Yajun Wang**[1], **Weibin Li**[1]

[1] *ZNDY Ministerial Key Laboratory, Nanjing University of Science and Technology, Nanjing 210094, China*
[2] *National Special Superfine Powder Engineering Research Center, Nanjing University of Science and Technology, Nanjing 210094, China*
* *E-mail:* njustlwb@163.com

Abstract: To improve the groove charge consistency and density and to reduce the initiation synchronicity error of a rigid multi-point initiation explosive network, a CL-20-based ultraviolet (UV)-curable high-explosive ink, comprising 42 wt.% sub-micron CL-20, a 55.4 wt.% binder system (including 2.0 wt.% NC and 53.4 wt.% butyl acetate), and 2.6 wt.% UV-curable resin, based on direct ink writing (DIW) technology, was prepared. The properties of the composite sample deposited via DIW were characterized. The results indicated that the sample had good uniformity, with few defects, and a critical detonation size of around 1.5×0.283 mm. A six-point initiation explosive network was designed for the integration of DIW technology and precise press-loading of the charge. The network featured six pre-pressed booster pellets with the same charge density ($\rho_0 = 1.89$ g·cm^{-3}, 95.8% of theoretical maximum density) as the output end charges, and a groove channel charged by DIW and press-loading. This procedure increased the density of the booster charge in the groove channels to 1.890 g·cm^{-3}, effectively improved the consistency of the charge density between the groove

channels and the output ends and lowered the initiation synchronicity error of the network to 62 ns. The network can initiate a jetting projectile charge (JPC) with good shape and small lateral offset, implying that the network initiation capability and synchronization meet the operational requirements of JPC shaped charges.

Keywords: multi-point initiation explosive network, UV-curability high-explosive ink, direct ink writing/printing, initiation synchronicity error, precise press-loading charge

1   Introduction

Shaped charges (SCs) have been extensively used in both military and civilian industry due to their great penetration capacity [1, 2]. The main goal of an SC designer is to obtain the maximum performance using the minimum high-explosive (HE) charge. A synchronous multi-point initiation (MPI) explosive network is often used in SCs to optimize the detonation wave and thus enhance the SCs ballistic performance without the need to change the warhead structure [3, 4]. An MPI explosive network is an explosives trace plate with a single-point input and a multi-point output. Unfortunately, there is always an error in the initiation synchronicity in an MPI explosive network, which affects the formation and penetration capability of the penetrator [5-7]. Therefore, minimization of the synchronicity error of the MPI explosive network applied to SCs is clearly required, and controlling the error makes considerable sense.

Many types of MPI systems already exist [8, 9], for example, the mild MPI explosive network, the electric MPI system, and the rigid MPI explosive network. Of these systems, the rigid MPI explosive network has the most widespread application in SCs, and features a complex network structure and many small-sized grooves. With limited machining accuracy, the explosive formulations and the groove charging methods are important factors affecting the synchronization of a rigid MPI explosive network. Researchers have prepared different polymer-bonded explosives [10-12] and proposed different charging methods, such as the silk screening technique [13], the micro-injection process [11, 12], and the press-loading charge method [9, 14]. Although there has been some progress, problems remain relating to charge density, charge consistency, initiation reliability, low sensitivity and synchronization. A new approach, direct ink writing (DIW), is now emerging. Compared with conventional groove charging methods, DIW is an attractive alternative for depositing

explosives in small groove channels due to its programmable material assembly technique. To date, researchers have made some progress in the formulation, properties and DIW execution for HE inks. However, the majority of the HE ink is fabricated and cured by thermal initiation polymerization, which is difficult to complete in a short time and has potential safety concerns in terms of operator handling [15-21]. Ultraviolet (UV)-curing technology is a high-speed phototreatment technology for liquid resin polymerization using a specific wavelength of UV-light for photoinitiator excitation [22]. This technology features rapid curing, safety, and excellent performance of the cured materials, and plays an important role in the fabrication of energetic materials, which is expected to be applicable in groove charging of a rigid MPI explosive network.

ε-2,4,6,8,10,12-Hexanitro-2,4,6,8,10,12-hexaazaisowurtzitane (CL-20) has been reported to have a high crystal density, high detonation velocity, excellent chemical and thermal stability, and good compatibility with the majority of binders [23, 24]. The critical diameter of CL-20 can reach the micron level, which is expected to be the requirement in small-sized explosive networks [11]. Moreover, research has shown that a decrease in the size of the explosive particles decreases the critical diameter and mechanical sensitivity, and increases the detonation wave propagation capability and safety of small groove charges [16, 25-26].

Here, in order to avoid heat curing during the DIW process, we have developed a sub-micron CL-20-based UV-curable suspension HE ink, which is deposited to produce an energetic composite by DIW. The related properties of the printed samples have been investigated and analyzed. Additionally, a rigid six-point initiation (SPI) explosive network was designed. The network was charged by DIW technology and a precise press-loading method with the prepared CL-20-based UV-curable HE ink. The network synchronization, explosion resistance capability, initiation capability, and SC live projectile test were also investigated in detail.

2   Preparation of CL-20-based UV-curable HE Ink and Ink Patterning

2.1 Materials

Raw CL-20 (ε phase) was provided by Liaoning Qingyang Special Chemical Co., Ltd. (Liaoyang, China). Nitrocellulose (NC, 12% N, industrial grade) was purchased from Foshan Junyuan Chemical Industry Co., Ltd. (Foshan, China). Ethanol and butyl acetate were obtained from Tianjin Guangfu Chemical

Industry Co., Ltd. (Tianjin, China). Epoxyacrylate (EA) and polyurethane acrylate (PUA) were from Nanjing Jinlu Chemical Industry Co., Ltd. (Nanjing, China). Trimethylolpropane triacrylate (TMPTA) and diphenyl(2,4,6-trimethylbenzoyl)phosphine oxide (TPO) were produced by Sarn Chemical Technology Co., Ltd. (Shanghai, China) and Shanghai Dibai Biotechnology Co., Ltd (Shanghai, China), respectively.

2.2 Preparation of sub-micron CL-20

Sub-micron CL-20 particles were prepared by milling. Approximately 100 g of pure raw ε-CL-20 was milled using a bidirectional rotary mill designed by the National Special Superfine Powder Engineering Research Center of China (Nanjing, China) with a liquid dispersant medium comprising ethanol and deionized water (having a volume ratio of 1:1). During the milling process, the suspension contained more than 70 wt.% deionized water and the temperature was less than 40 °C. After 5 h of milling, the slurry was filtered, washed with water and freeze dried, and sub-micron CL-20 samples were obtained.

2.3 Preparation of UV-curable resin and CL-20-based HE ink

A UV-curable resin was added to the formulation of the HE ink, so that the ink written in the grooves could be cured rapidly by irradiation with UV light. This prevented the flow of the HE ink and ensured the consistency of the groove charge. The UV-curable resin was prepared as follows (Figure 1(a)): Initially, 2.0 wt.% TPO, 4.0 wt.% TMPTA and 6.0 wt.% ethanol were mixed in a beaker with a mechanical stirrer at 100 rpm for 60 min at room temperature. Then 78.0 wt.% EA and 10.0 wt.% PUA were dissolved in the above solution and stirred evenly for 2 h.

The preparation of the CL-20-based UV-curable HE ink (Figure 1(b)) was as follows:

– Initially, 2.0 wt.% NC and 2.6 wt.% of the prepared UV-curable resin were added and stirred into 53.4 wt.% butyl acetate solution at 100 rpm for 2 h at room temperature.
– Secondly, 42.0 wt.% of the prepared sub-micron CL-20 sample was added to the solution and left to stir for a further 4 h at 50 rpm, followed by ultrasonication at 20 kHz for 30 min.
– A milky-white suspension, the CL-20-based UV-curable HE ink, was obtained, with relatively low viscosity and desirable stability.
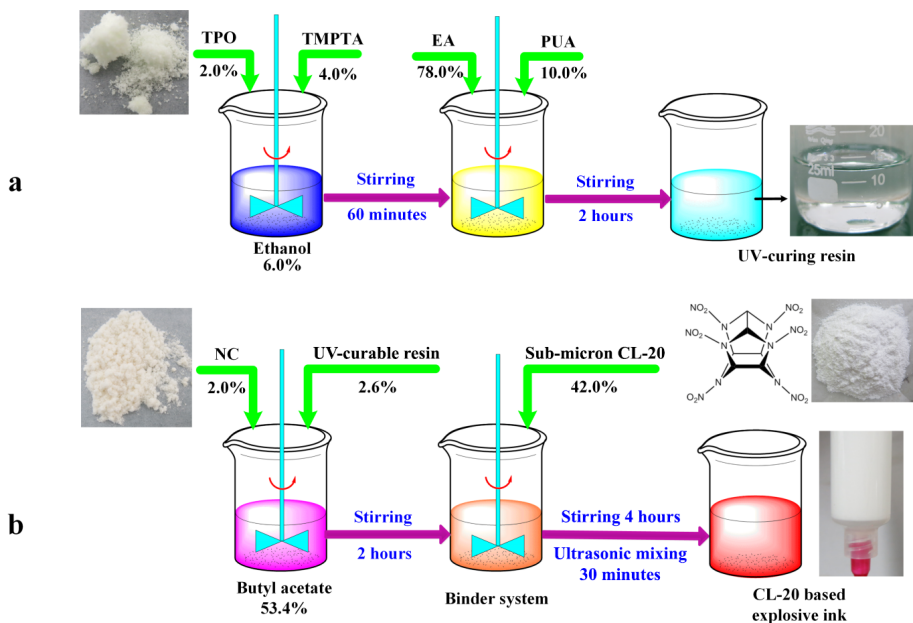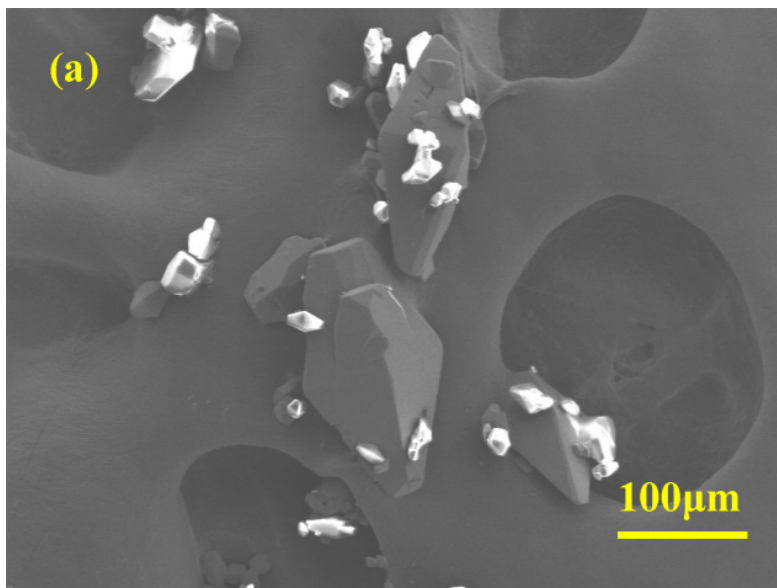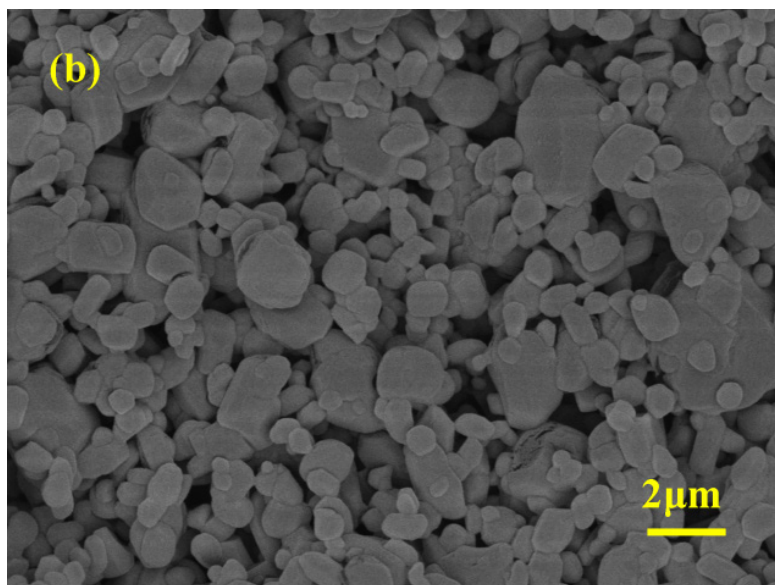– Finally, the prepared HE ink was housed in a syringe for ink patterning.

Figure 1. Sample preparation: (a) UV-cured resin and (b) CL-20-based UV-cured HE ink
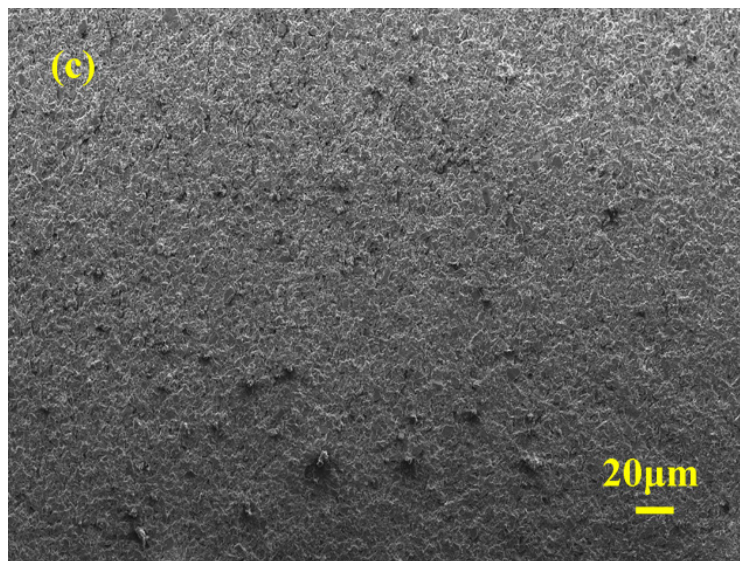
2.4 Ink patterning

The DIW system, which comprises an MC400 three-dimensional (3D) motion platform (Beijing Zolix Instruments Co. Ltd., Beijing, China), an Ultra 2400 dispenser (Nordson EFD, USA), and a UVEC-4 ultraviolet light (Shenzhen Lamplic Technology Co., Ltd., Shenzhen, China), was used to print and deposit the CL-20-based UV-curable HE ink. Figure 2 is a schematic diagram of DIW, where instructional scheduled programs (3D motion control program and gas on-off control program) were applied to control the movement of the motion platform and the on-off state of the dispenser. During manufacture, the shape of the product is determined by the scheduled program of the motion platform and the on-off state of gas through which inks were printed and deposited onto grooves or substrates. The deposited ink was cured and patterned under the irradiation of ultraviolet light. After curing, and the CL-20-based composites had been fabricated, the pattern structures were freed of the remaining solvent for 24 h at 45 °C and −0.08 MPa in a vacuum oven.
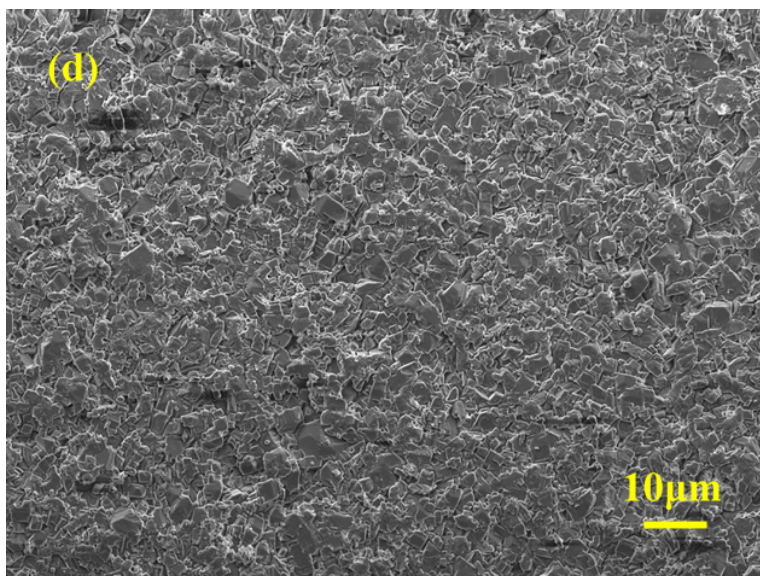
Figure 2.   Direct ink writing

3   Sample Characterization and Properties

3.1 Characterization of the morphology

Initially the ink was deposited on a steel substrate to test the functioning and stability of the CL-20-based UV-curable HE ink. The morphologies of the raw CL-20, sub-micron CL-20, and post-cured CL-20-based composite (Figure 3) were examined using an S-4800 scanning electron microscope (SEM, Hitachi, Ltd., Kyoto, Japan). Figure 3(a) shows that the particle shapes of raw CL-20 was mostly polyhedral, and the particle size was 80 to 150 μm. Figure 3(b) shows that the sub-micron CL-20 particles are 1 to 10 μm pseudo-spheres with a smooth surface after 5 h of wet ball milling. The morphologies of the post-cured CL-20-based composite, shown in Figures 3(c) and 3(d), show the smooth exterior surfaces and the compact particle network that comprises each element during the assembly and drying processes. There were no faults, such as cracks, porosities, voids, and the like, in the composite, which is advantageous for the uniformity of the charge density and better safety and performance.

(a)

(b)

(c)

(d)

Figure 3.   SEM images of raw CL-20 (a), sub-micron CL-20 (b), and the printed CL-20-based composite (c, d)

3.2 XRD characterization

The usefulness of the CL-20-based HE ink patterning in an MPI explosive network is highly d ependent on the crystal polymorph. The raw CL-20, sub-micron CL-20, and post-cured CL-20-based composite were therefore characterized by X-ray diffraction (XRD). The XRD patterns (Figure 4) were recorded using a D8 Advance diffraction system (Bruker, Germany) with Cu-Ka (λ = 1.540598 Å) radiation at 40 kV and 30 mA. Figure 4 shows that the three strong diffraction peaks of raw CL-20, sub-micron CL-20, and the CL-20-based composite are basically the same. The diffraction angles $2\theta = 12.6°$, $13.8°$ and $30.3°$ correspond to the (11-1), (200) and (20-3) crystal faces of ε-CL-20, which are in agreement with the standard PDF card (00-050-2045) of ε-CL-20. The test results demonstrated that the milling, mixing, patterning and curing processes do not affect the form of ε-CL-20, which has a high energy density, high detonation velocity, and excellent chemical stability.
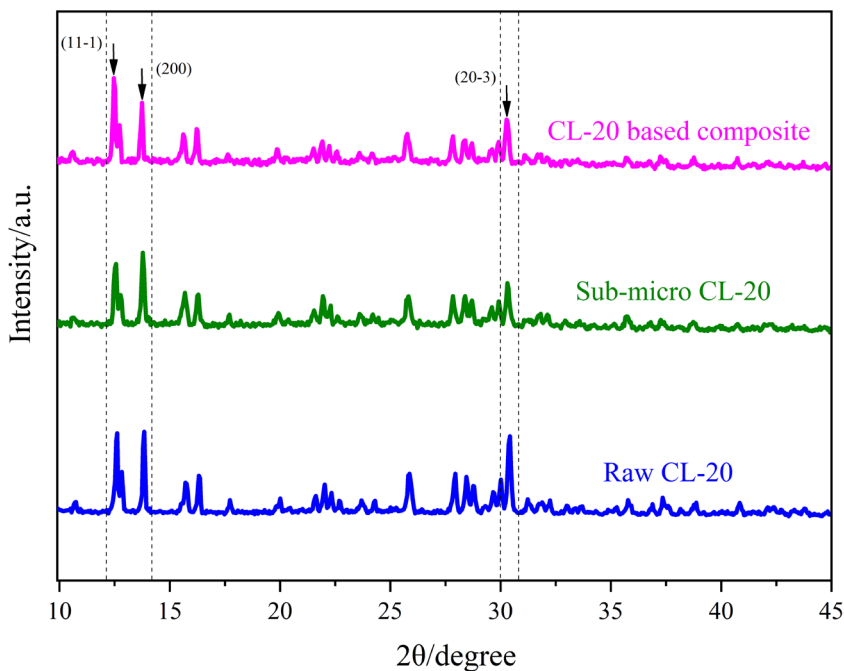

Figure 4.   XRD diffraction patterns of raw CL-20, sub-micron CL-20, and the CL-20-based composite

3.3 Critical size of detonation

The critical size of detonation was tested by loading the CL-20-based UV-curable HE ink into a wedge groove of a strip plate made of 45# steel (Figure 5). The groove had length $L_0 = 150$ mm, width 1.5 mm, and deepest side $H_0 = 3$ mm. The wedge groove charge was initiated by an 8# detonator.
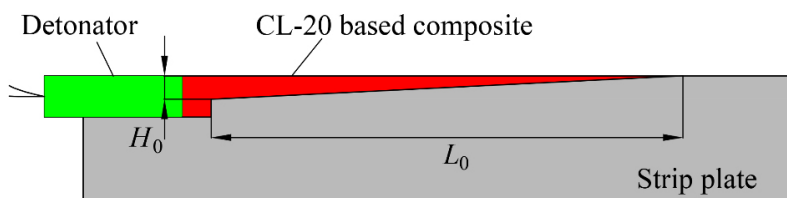

Figure 5.   Wedge-shaped charge testing device

The critical size of detonation (H_c) can be calculated as [19, 20]:

$$H_c = \frac{H_0 \times (L_0 - L_c)}{L_0} \tag{1}$$

where L_c is the length of the explosion track, which was 135.84 mm, as shown in Figure 6. The critical size of detonation H_c can therefore be calculated using Equation 1 as 0.283 mm, which indicates that the post-cured CL-20-based composite can be detonated steadily above 1.5×0.283 mm.
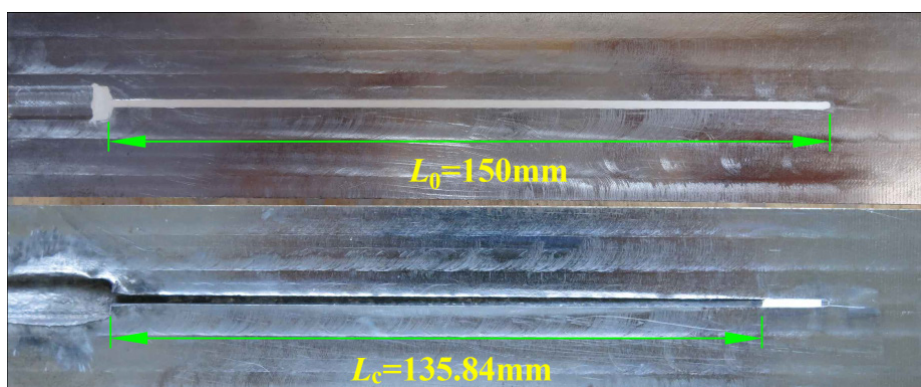

Figure 6.   Wedge-shaped charge test: (top) pre-detonation, (bottom) post-detonation

3.4 Density of the composite

In the field of energetic materials, density is an important parameter affecting the detonation properties. Given that the HE ink is commonly applied in small groove channels, the printed density should be as high as possible. To obtain the desired explosive effect along the initiation train, a charge density greater than 90% of theoretical maximum density (TMD) is generally required [21]. The TMD of the post-cured CL-20-based composite (ρ_{TMD}) can be calculated using the Urizar method (volume plus method) as [27]:

$$\rho_{\text{TMD}} = \frac{\sum m_{\text{i}}}{\sum \left(m_{\text{i}} / \rho_{\text{i,TMD}} \right)} \tag{2}$$

where m_{i} is the mass of an ingredient i (g) and $\rho_{\text{i,TMD}}$ is the TMD of the ingredient i (g·cm^{-3}).

The post-cured CL-20-based composite was removed from five different positions along the wedge-shaped groove (Figure 6) and the printed charge density was then measured (see Table 1) using an MH-300A high-precision electronic densimeter (Xiamen Yishite Instruments Co., Ltd., Xiamen, China) having a testing accuracy of 0.001 g·cm^{-3}. Table 1 shows that the standard deviation (σ) of the printed density was small, indicating that the charge uniformity and consistency was good for DIW. The table also shows that the average printed density of the CL-20 based composite was 1.297 g·cm^{-3}, which is only 65.7% of the TMD, lower than the 90% requirement. This means that the printed density of the CL-20-based composite is low, and measures should be taken to increase the charge density when the composite is applied for the groove charging of an MPI explosive network.

Table 1.   TMD and initial printed density of CL-20 based composite

TMD [g·cm^{-3}]	Measured density [g·cm^{-3}]						
	1	2	3	4	5	Average	σ
1.973	1.305	1.293	1.302	1.291	1.295	1.297	0.006

4   Explosive Network Charge and Performance Test

4.1 Explosive network structure

A rigid synchronous SPI explosive network was designed on the basis of the experimental results of the detonation critical size and earlier research on MPI penetrator formation and MPI explosive network designs [5-7]. The network comprised a parent plate with six grooves. The plate was made of 45# steel and had diameter 100 mm and thickness $H = 6$ mm. Six rectangular grooves, of length $R = 30$ mm, width $w = 1.5$ mm and depth $d = 2.0$ mm, emanate radially from the center (see Figure 7).
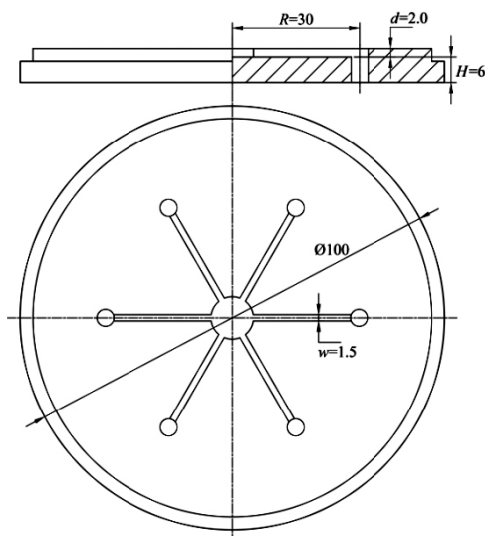
Figure 7.   Structure of the SPI explosive network (units: mm)

4.2 Charging of the explosive network

Research has shown that, with limited machining accuracy for the network grooves, increasing the detonation velocity and decreasing the variation of the detonation velocity of the booster explosive can effectively reduce the error in the initiation synchronicity of the MPI explosive network [8, 28]. The detonation velocity (D) and the charge density (ρ_0) satisfy the relation [27]:

$$D = \frac{D_{max}}{4} + \frac{3}{4}\frac{D_{max}}{\rho_{TMD}}\rho_0 \tag{3}$$

where D_{max} and ρ_{TMD} are the theoretical detonation velocity and TMD of the composite explosive, respectively. It can be seen from Equation 3 that increasing the booster charge density ρ_0 increases the detonation velocity D, and thus can reduce the error in the network initiation synchronicity. For a certain explosive network, the variation in the detonation velocity is related to the uniformity and consistency of the network groove charge [8]. For this purpose, in developing the charging of the explosive network groove, the DIW technology was used to deposit the CL-20-based UV-curable HE ink in the network grooves, and the ink in the grooves was cured under ultraviolet irradiation. The network then was placed in a vacuum oven (-0.08 MPa) and freed of solvent for 24 h at 45 °C. After drying the cured deposited ink in the network grooves, a specially designed pressing mold was used for pressing the groove charge to increase its charge density (see Figure 8).
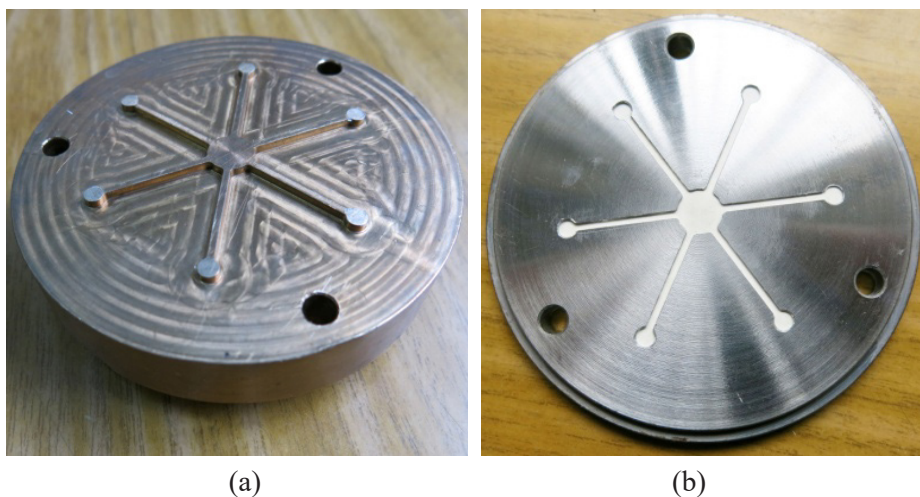

(a)   (b)

Figure 8.   Pressing mold (a) and (b) of the pressed SPI explosive network

4.3 Synchronization

The initiation synchronicity error of the MPI explosive network strongly affects the formation and penetration capability of the penetrator [5-7]. It is therefore necessary to validate the synchronization of the designed SPI explosive network. The initiation synchronicity error was measured using a PXI-1412 timing test system (ADLINK Technology (China), Co., Ltd., Shanghai, China) having a testing accuracy of 2 ns. Seven ionization probes labeled 0#, 1#, 2#, 3#, 4#, 5#, and 6# were used to indicate the action times of the pressed SPI explosive network (see Figure 9).
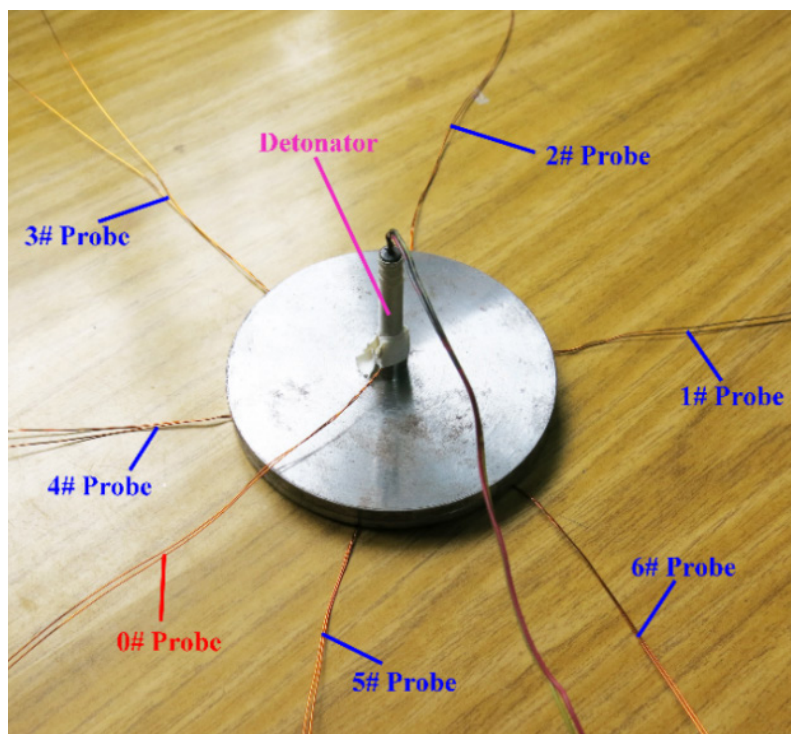
Figure 9.   Measurement of the synchronization of the SPI explosive network

Figure 9 shows that the 0# probe is firmly fixed to the 8# detonator, and the other six probes are closely placed on the network output end face. After activation of the 8# detonator, the 0# probe generates a starting trigger signal. As the detonation wave propagates to the six-output ends, the 1#, 2#, 3#, 4#, 5#, and 6# probes produce terminal trigger signals. The action times between the start signal and terminal signals were recorded by the PXI-1412 timing test system. The lowest of the six action times was used as the standard value, and the others were compared with the standard value to obtain the relative times in Table 2, *i.e.* the initiation synchronicity error of the pressed SPI network.

Table 2.   Initiation synchronicity error of the pressed SPI explosive network

n	Action time [ns]						Synchronicity error [ns]					
	t_1	t_2	t_3	t_4	t_5	t_6	Δt_1	Δt_2	Δt_3	Δt_4	Δt_5	Δt_6
1	5824	5832	5958	5876	5904	5838	0	8	134	52	80	14
2	5814	5830	5942	5862	5926	5840	0	16	128	48	112	26
3	5802	5816	5814	5818	5856	5938	0	14	12	16	54	138

Analyzing the results in Table 2, it can be observed that the deviation time of the network varies and the maximum value of the initiation synchronicity error was 138 ns. When measuring the network synchronization by the ionization probe method, an SIM-type ultra-high-speed camera (Specialised Imaging Ltd., Pitstone, UK) was used to capture light emission from the six output ends (Figure 10, corresponding to experiment number $n = 3$ in Table 2). The maximum exposure speed of the camera was $6 \cdot 10^6$ fps, with an exposure time of 60 ns and an interval between images of 20 ns. The phases of the six output end light emissions shown in Figure 10 are inconsistent, which implies that the synchronization of the pressed SPI explosive network is poor.

$t = 5.86$ μs $t = 5.94$ μs

$t = 6.02$ μs $t = 6.10$ μs
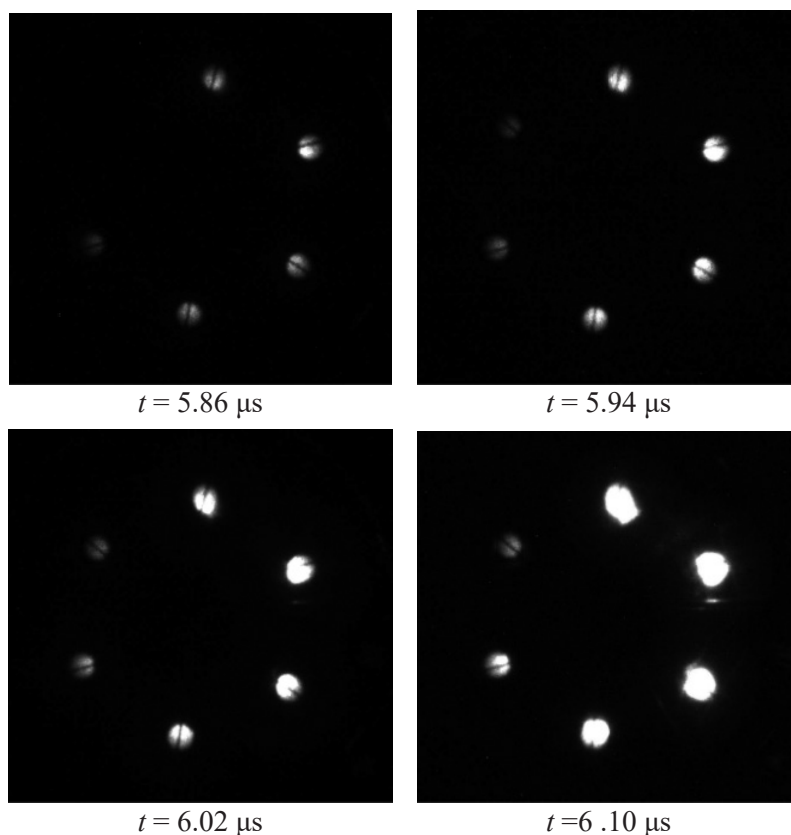
Figure 10. Evolution of the light emissions of the six output ends (for experiment $n = 3$ in Table 2)

4.4 Charge density

The cured charge was removed from the six groove channels and the six output ends of the pressed SPI explosive network, respectively, and then the charge density was measured (see Table 3). The results shown in Table 3 show the average density of the groove channel charges after pressing (*viz.* 1.890 g·cm^{-3}) was 95.8% of the TMD, whereas at the output ends (*i.e.* 1.389 g·cm^{-3}), it was only 70.4%. The groove charge density was increased by 45.7% after pressing, whereas at the output end by only 7.1%, compared with the composite printed charge density shown in Table 1. The charge density in the groove channels and the output ends exhibited an inconsistency which contributed to the poor network synchronization.

Table 3. Density of CL-20 based composite in the groove channels and output ends

Position	TMD [g·cm^{-3}]	Measured density [g·cm^{-3}]							
		1	2	3	4	5	6	Average	σ
Groove channels	1.973	1.891	1.885	1.887	1.888	1.902	1.886	1.890	0.006
Output ends	1.973	1.403	1.397	1.401	1.384	1.379	1.370	1.389	0.013

5   Optimization and Performance of the Explosive Network

5.1 Explosive network optimized

It was known from Section 4.4 that the inconsistencies in the densities in the groove channel and output-ends, and lower charge density of the output ends contributed to the poor synchronization of the pressed SPI explosive network. In order to reduce the error in the network synchronicity and to improve charge consistency, we optimized the SPI explosive network charge structure as shown in Figure 11:

– Firstly, the CL-20-based UV-curable HE ink cured by ultraviolet irradiation was placed in a vacuum oven (−0.08 MPa) and dried for 24 h at 45 °C.
– Secondly, the post-cured CL-20-based composite explosive was pre-pressed into six 6.5(Φ)×6.0 mm cylindrical booster pellets with the same density (ρ_0 = 1.89 g·cm^{-3}, about 95.8% of the TMD, Figure 11(f)), which were used as the output end charges of the SPI explosive network (Figure 11(e)).

–   Thirdly, DIW technology was used to deposit the CL-20-based UV-curable HE ink into the six groove channels, and the ink in the grooves was cured under ultraviolet irradiation.

–   Then the network was placed in a vacuum oven (−0.08 MPa) and dried for 24 h at 45 °C.

–   Finally, a special pressing mold (Figure 11(c)) was used to press the cured groove channel charges and increase the charge density to 1.890 g·cm^{-3} (Figure 11(b)), and to make the groove channel charge density consistent with the density of the pre-pressed booster pellets.
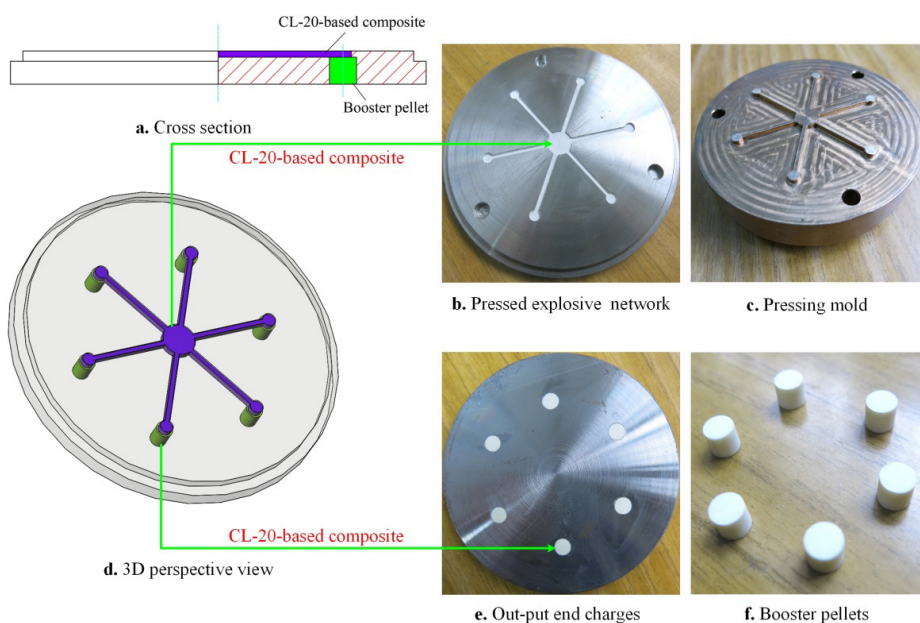
Figure 11. Charge structure of the optimized SPI explosive network and pressing mold

5.2 Synchronization

In the same manner, the synchronization of the optimized SPI explosive network (Figure 11) was investigated using the timing test system and the ultra-high-speed camera. The results listed in Table 4 and Figure 12 show the initiation synchronicity error and evolution of the six output end light emissions (corresponding to experiment $n = 3$ in Table 4) of the optimized SPI explosive network.
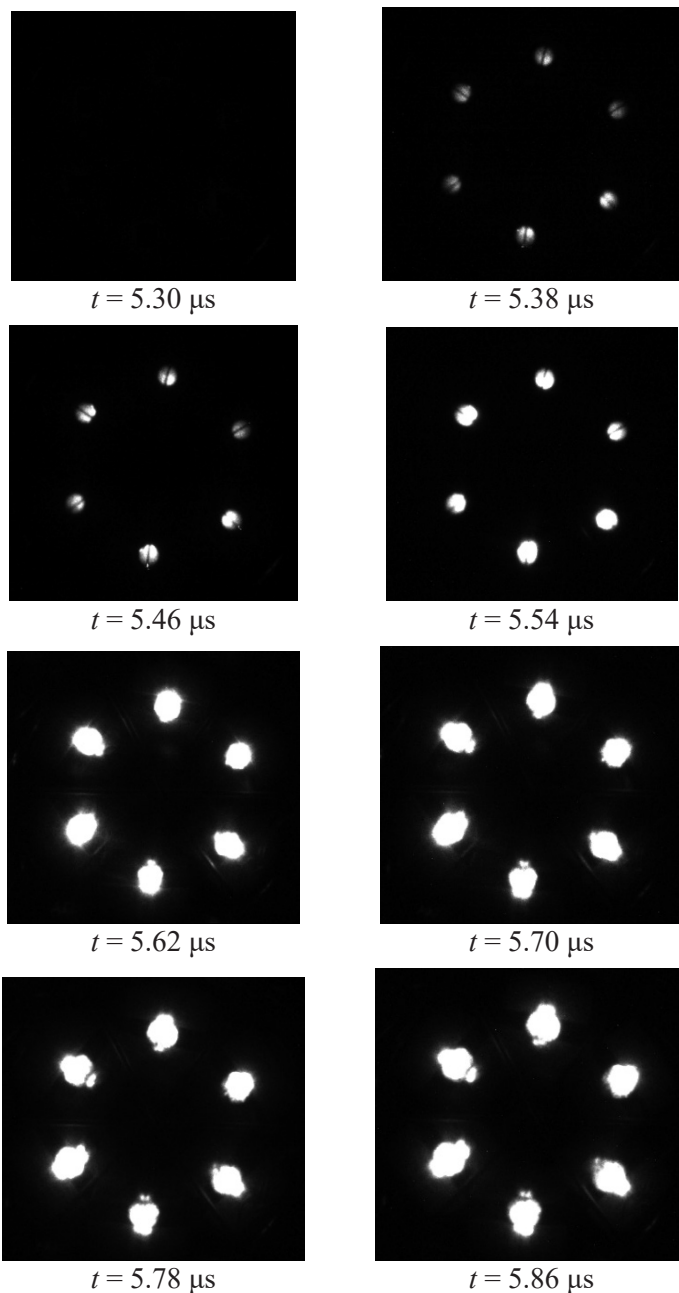
$t = 5.30$ μs

$t = 5.38$ μs

$t = 5.46$ μs

$t = 5.54$ μs

$t = 5.62$ μs

$t = 5.70$ μs

$t = 5.78$ μs

$t = 5.86$ μs

Figure 12. Evolution of the light emissions of the six output ends (for experiment number $n = 3$ in Table 4)

Table 4.   Initiation synchronicity error in the optimized SPI explosive network

n	Action time [ns]						Synchronicity error [ns]					
	t_1	t_2	t_3	t_4	t_5	t_6	Δt_1	Δt_2	Δt_3	Δt_4	Δt_5	Δt_6
1	5296	5328	5354	5316	5314	5330	0	32	58	20	18	34
2	5302	5352	5344	5364	5330	5312	0	50	42	62	28	10
3	5308	5318	5368	5330	5338	5354	0	10	60	22	30	46

Analysis of the results in Figure 12 reveals that there is no light emission at time $t = 5.30$ μs and six light emissions at $t = 5.38$ μs, implying that the synchronicity error of the optimized SPI explosive network is less than 80 ns. The test results in Table 4 show that the maximum error is 62 ns, which is less than the previous test results in Section 4. The pre-pressed booster pellets were thus used as the output end charges, and the DIW technology was applied for groove channel charging, ensuring the consistency of the network groove channel charges. The pressing mold was employed to increase the groove channel charge density and to eliminate the air gap between the groove channel charges and booster pellets, ensuring the consistency of the groove channel charges and booster pellets. Therefore, using this optimized network charge structure, consistency of the charge density and the propagation reliability of the detonation wave were enhanced, improving the network synchronization.

5.3 Explosion resistance

The optimized SPI explosive network (Figure 11) used in a warhead is to simultaneously realize SPI of the main charge. The shock wave, generated by the groove charge explosion, propagated and attenuated in the network parent plate should not initiate the warhead main charge, which therefore requires the network parent plate to have a certain thickness and its explosion resistance to be effective. A $15(\Phi)\times10$ mm cylindrical JH-2 (RDX-based explosive, $\rho_0 = 1.70$ g·cm^{-3}) HE charge was therefore placed on a steel witness plate (Figure 13). An optimized SPI explosive network (Figure 13, charge structure as Figure 11 and Section 5.1) was then placed on the JH-2 HE charge. After the action of an 8# detonator on the network, the results (Figure 13) showed a white powder mark remaining on the network parent plate and the witness plate, demonstrating that the JH-2 HE charge was not initiated, indicating that the explosion resistance of the 6-mm 45# steel parent plate was effective.
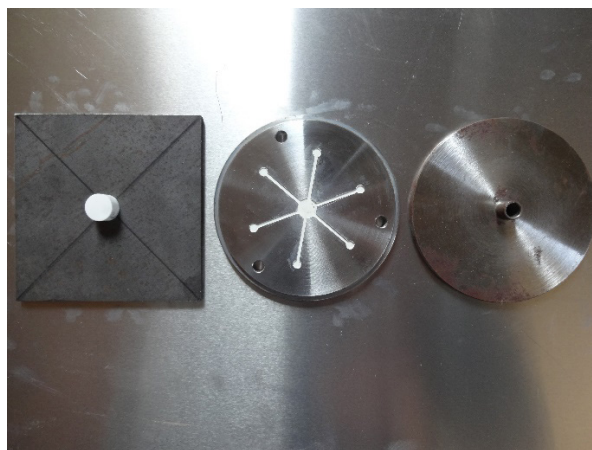
(a)
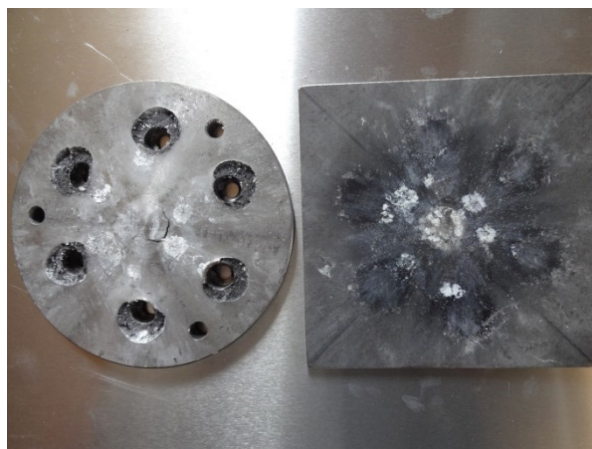
(b)

Figure 13. Parent plate explosion resistance validation: (a) pre-detonation, and (b) post-detonation

5.4 Initiation capability

To facilitate a capability test of the initiation of the optimized SPI explosive network (Figure 11), six $10(\Phi)\times10$ mm cylindrical JH-2 HE charges ($\rho_0 = 1.70$ g·cm^{-3}) were firmly fixed on the output end face centres of the optimized SPI explosive network (Figure 14). The charges were then fastened onto a steel witness plate. Following initiation by an 8# detonator, the six dents generated on the steel witness plate (Figure 14) revealed that the optimized SPI explosive network initiation capability is reliable.
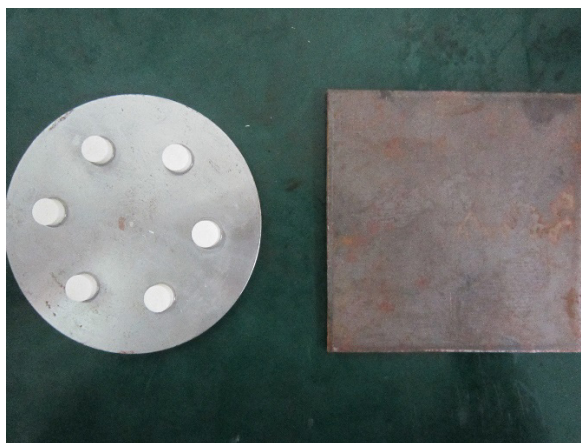
(a)

(b)

Figure 14. Validation of the optimized SPI explosive network initiation capability: (a) pre-detonation, and (b) post-detonation

5.5 Live projectile test

In order to investigate the initiation capability and synchronization of the optimized SPI explosive network (Figure 11), a jetting projectile charge (JPC) SC (Figure 15) was matched with the optimized SPI explosive network in a live projectile test. The JPC SC consisted of JH-2 HE (ρ_0 = 1.70 g·cm^{-3}) with an eccentric sub-hemisphere liner. The length (L_c) and diameter (D_c) of the JH-2 HE charge were 90 and 100 mm, respectively. The liner was made of pure copper, of dimensions shown in Figure 15. Two 450 kV Scandiflash flash X-ray systems

(Scandiflash AB, Uppsala, Sweden) were employed to obtain the penetrator formation images, from which the parameters of the penetrator, such as formation, length (L), diameter (D), and average velocity (V_{av}) of the penetrator tip and tail, can be obtained.
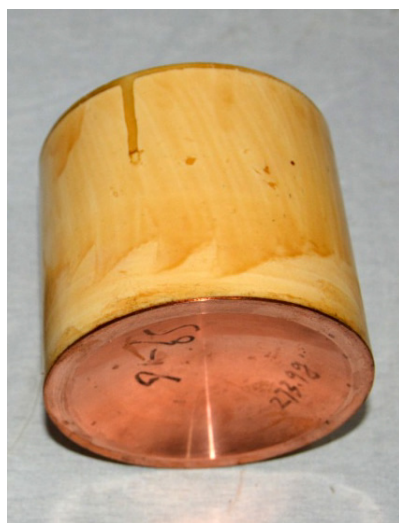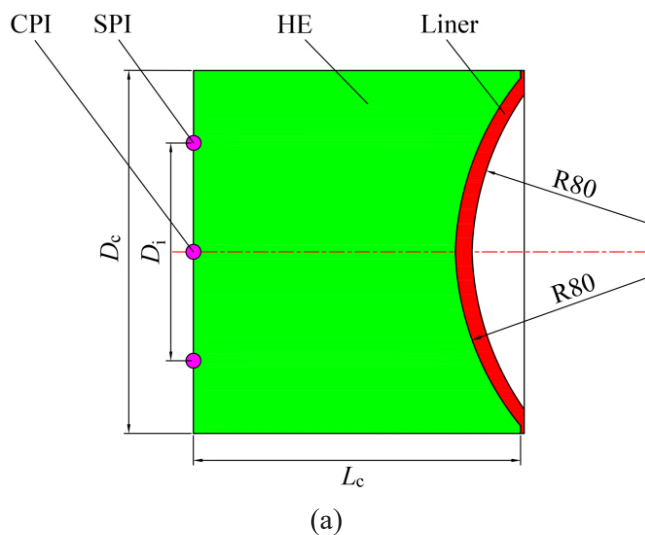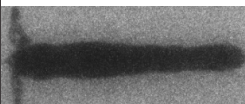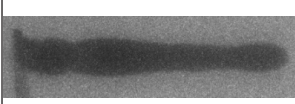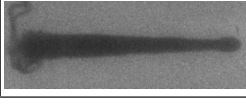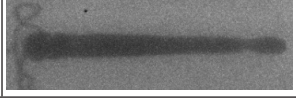

(a)

(b)

Figure 15. JPC SC: (a) cross section (units: mm) and (b) photographic view

The results in Table 5 show the JPC formation parameters at times $t = 150$ μs and $t = 180$ μs for two initiation projects: center point initiation (CPI) and SPI. Analyzing the penetrator shape obtained from the X-ray photographs, it can be found that the JPC was stretched into a longer rod-like shape with SPI. The length-to-diameter ratio (L/D) and average tip velocity of the penetrator was increased approximately 98.8% and 25.6% from the CPI to the SPI project, at time $t = 180$ μs. The increase in the L/D ratio and tip velocity is an advantage for JPC penetration. Note also that the optimized SPI explosive network forms a JPC with good shape and small lateral offset, implying that the initiation capability and synchronization of the optimized network meet the operational requirements of the JPC SCs.

Table 5.　　JPC formation for two different initiation projects

Project	$t = 150$ μs		$t = 180$ μs		V_{av} [m/s]	
	Penetrator shape	L/D	Penetrator shape	L/D	tip	tail
CPI		7.5		8.3	2177	1676
SPI		15.2		16.5	2735	1756

6　Conclusions

♦ The integration of DIW technology and explosive materials was investigated. A CL-20-based UV-curable HE ink, composed of:
  – 42 wt.% sub-micron CL-20,
  – 2.0 wt.% NC,
  – 53.4 wt.% butyl acetate,
  – and 2.6 wt.% UV-curable resin (including 78 wt.% EA, 10 wt.% PUA, 2 wt.% TPO, 4 wt.% TMPTA, and 6 wt.% ethanol)
  was prepared and deposited to obtain CL-20-based composites.
♦ The properties of the CL-20-based composite were characterized by XRD and SEM. The results showed that the crystal polymorph of ε-CL-20 was not changed, the CL-20-based composite had good uniformity without cracks, porosities and voids, and that the critical size of detonation was around 1.5×0.283 mm. The printed density of the composite was about 1.297 g·cm^{-3}, which is 65.7% of the TMD.

- ♦ Six 6.5(Φ)×6.0 mm pre-pressed cylindrical CL-20-based composite booster pellets with the same density ($\rho_0 = 1.89$ g·cm^{-3}, 95.8% of the TMD) were used as output-end charges of an SPI explosive network. The DIW technology was used to deposit the CL-20-based UV-curable HE ink into the network groove channels to realize groove booster charging. A precise press-loading method was used to increase the density of the booster charge in the groove channels to 1.890 g·cm^{-3}, so that it matched the density for the pre-pressed booster pellets. In effect, this improves the charging density consistency and reduces the initiation synchronicity error of the network to 62 ns.
- ♦ The explosion resistance and initiation capability of the designed SPI explosive network were effective and reliable. The optimized SPI network was matched with a JPC SC in a live projectile test. These test results showed that the tip velocity and L/D ratio of the JPC were about 1.26 and twice as large as a CPI test. The network is expected to form a JPC with small lateral offset and good shape, thereby meeting the network application requirements of JPC SCs.

Acknowledgments

References

[1] Xu, W.L.; Wang, C.; Chen, D.P. Formation of a Bore-center Annular Shaped Charge and Its Penetration into Steel Targets. *Int. J. Impact. Eng.* **2019**, *127*: 122-134.

[2] Xu, W.L.; Wang, C.; Chen, D.P. The Jet Formation and Penetration Capability of Hypervelocity Shaped Charges. *Int. J. Impact. Eng.* **2019**, *132*: 103337.

[3] Ellis, J. *Shaped-charge with Simultaneous Multi-point Initiation of Explosives*. Patent US 5479860, **1996**.

[4] Daniels, A.S.; Baker, E.L.; Vuong, T.H.; Chin, C.L.; Fuchs, B.F.; Defisher, S.E. Selectable Initiation Shaped Charges. *20th Int. Symp. on Ballistics*, Florida, USA, **2002**, 679-684.

[5] Li, R.; Li, W.B.; Wang, X.M.; Li, W.B. Effects of Control Parameters of Three-point Initiation on the Formation of an Explosively Formed Projectile with Fins. *Shock Waves* **2018**, *28*(2): 191-204.

[6] Li, W.B.; Wang, X.M.; Li, W.B. The Effect of Annular Multi-point Initiation on the Formation and Penetration of an Explosively Formed Penetrator. *Int. J. Impact. Eng.* **2010**, *37*(4): 414-424.

[7] Li, R.; Li, W.B.; Guo, X.D.; Liang, L.; Li, W.B.; Wang, X.M. Effect of the Annular Multi-point Initiation Control Parameters on Jet Formation. *Propellants Explos. Pyrotech*. **2019**, *44*: 127-137.

[8] Li, Y.; Li, Y.H.; Wen, Y.Q. A Method for Estimating the Synchronization of a Mild Multipoint Synchronous Initiation Circuit. *J. Energ. Mater*. **2018**, *36*(2): 152-168.

[9] Hu, L.S.; Hu, S.Q.; Cao, X. Study on the Initiation Capacities of Two Booster Pellets. *Cent. Eur. J. Energ. Mater.* **2012**, *9*(2): 261-272.

[10] Wang, J.Y.; An, C.W.; Li, G.; Liang, L.; Xu, W.Z.; Wen, K. Preparation and Performances of Castable HTPB/CL-20 Booster Explosives. *Propellants Explos. Pyrotech*. **2011**, *36*: 34-41.

[11] Wei, Y.J.; Wang, J.Y.; An, C.W.; Li, H.Q.; Wen, X.M.; Yu, B.S. GAP/CL-20-based Compound Explosive: A New Booster Formulation Used in a Small-sized Initiation Network. *J. Energ. Mater.* **2017**, *35*(1): 53-62.

[12] An, C.W.; Wen, X.M.; Wang, J.W.; Wu, B.D. GAP/DNTF Based PBX Explosives: A Novel Formula Used in Small Sized Explosive Networks. *Cent. Eur. J. Energ. Mater.* **2016**, *13*(2): 397-410.

[13] Gibbons, G.; Silvia, D.A. *Manufacture of Explosive Networks using Silk Screening Techniques and Explosive Inks*. Patent US 5046425, **1991**.

[14] Xue, Z.Q.; Hu, S.Q.; Cao, X.; Zhang, J. A Study of the Detonation Behavior of an Annular Booster Pellet. *J. Energ. Mater.* **2017**, *35*(1): 9-19.

[15] Ihen, A.; Lee, W.; Fuchs, B.; Petrock, A.; Samuels, P.; Stepanov, V.; Stasio, A.D. Inkjet-printing of Nanocomposite High-explosive Materials for Direct Write Fuzing. *54th Fuze Conf.*, Kansas City, MO, **2010**, 11-13.

[16] Wang, D.J.; Zheng, B.H.; Guo, C.P.; Gao, B.; Wang, J.; Yang, G.C.; Huang, H.; Nie, F.D. Formulation and Performance of Functional Sub-micro CL-20-based Energetic Polymer Composite Ink for Direct-Write Assembly. *RSC Adv*. **2016**, *6*: 112325-112331.

[17] Xu, C.H.; An, C.W.; Li, Q.B.; Xu, S.; Wang, S.; Guo, H.; Wang, J.Y. Preparation and Performance of Pentaerythrite Tetranitrate-based Composites by Direct Ink Writing. *Propellants Explos. Pyrotech*. **2018**, *43*: 1149-1156.

[18] Xu, C.H.; An, C.W.; He, Y.N.; Zhang, Y.R., Li, Q.B.; Wang, J.Y. Direct Ink Writing of DNTF Based Composite with High Performance. *Propellants Explos. Pyrotech*. **2018**, *43*: 754-758.

[19] Wang, J.Y., Xu, C.H.; An, C.W.; Song, C.K.; Liu, B.; Wu, B.D.; Geng, X.H. Preparation and Properties of CL-20 Based Composite by Direct Ink Writing. *Propellants Explos. Pyrotech*. **2017**, *42*: 1139-1142.

[20] Li, Q.B.; An, C.W; Han, X.; Xu, C.H.; Song, C.K.; Ye, B.Y.; Wu, B.D.; Wang, J.Y. CL-20 Based Explosive Ink of Emulsion Binder System for Direct Ink Writing. *Propellants Explos. Pyrotech*. **2018**, *43*: 533-537.

[21] Xu, C.H.; An C.W.; Long Y.L.; Li Q.B.; Guo H.; Wang S.; Wang J.Y. Inkjet Printing of Energetic Composites With High Density. *RSC Adv*. **2018**, *8*: 35863-35869.

[22] Decker, C. Kinetic Study and New Applications of UV Radiation Curing. *Macromol. Rapid Commun.* **2002**. *23*: 1067-1093.

[23] Nair, U.R.; Sivabalan, R.; Gore, G.M.; Geetha, M.; Asthana, S.N.; Singh, H. Hexanitrohexaazaisowurtzitane (CL-20) and CL-20-based Formulations (review). *Combust. Explo. Shock*. **2005**, *41*(2): 121-132.

[24] Cumming, A.S. New Trends in Advanced High Energy Materials. *J. Aero. Tech. Manag*. **2009**, *1*(2): 161-166.

[25] Kobylkin, I.F. Critical Detonation Diameter of Highly Desensitized Low-sensitivity Explosive Formulations. *Combust. Explo. Shock*. **2009**, *45*(6): 732-737.

[26] An, C.W.; Li, H.Q.; Guo, W.J.; Geng, X.H.; Wang, J.Y. Nano Cyclotetramethylene Tetranitramine Particles Prepared by a Green Recrystallization Process. *Propellants Explos. Pyrotech*. **2014**, *39*: 701-706.

[27] Dobratz, B.M.; Crawford, P.C, *LLNL Explosives Handbook Properties of Chemical Explosives and Explosive Simulants*. Lawrence Livermore National Laboratory, Livermore, CA, **1985**, pp. 8-13.

[28] Hu, L.S.; Hu, S.Q.; Cao, X. Application of the Multipoint Synchronous Circuit of the Annular Booster Pellet. *Int. J. Energ. Mater. Chem. Prop*. **2013**, *12*(6): 475-485.